JACS
JOURNAL OF THE AMERICAN CHEMICAL SOCIETY

Article

pubs.acs.org/JACS

Quinoxaline-Based Polymer Dots with Ultrabright Red to Near-Infrared Fluorescence for In Vivo Biological Imaging

Hong-Yi Liu,[†] Pei-Jing Wu,[†] Shih-Yu Kuo,[†] Chuan-Pin Chen,[†] En-Hao Chang,[†] Chang-Yi Wu,[‡] and Yang-Hsiang Chan*[,†]

[†]Department of Chemistry, National Sun Yat-sen University, 70 Lien Hai Road, Kaohsiung, Taiwan 80424

[‡]Department of Biological Sciences, National Sun Yat-sen University, 70 Lien Hai Road, Kaohsiung, Taiwan 80424

Supporting Information

ABSTRACT: This article describes the design and synthesis of quinoxaline-based semiconducting polymer dots (Pdots) that exhibit near-infrared fluorescence, ultrahigh brightness, large Stokes shifts, and excellent cellular targeting capability. We also introduced fluorine atoms and long alkyl chains into polymer backbones and systematically investigated their effect on the fluorescence quantum yields of Pdots. These new series of quinoxaline-based Pdots have a fluorescence quantum yield as high as 47% with a Stokes shift larger than 150 nm. Single-particle analysis reveals that the average per-particle brightness of the Pdots is at least 6 times higher than that of the commercially available quantum dots. We further demonstrated the use of this new class of quinoxaline-based Pdots for effective and specific cellular and subcellular labeling without any noticeable nonspecific binding. Moreover, the cytotoxicity of Pdots were evaluated on HeLa cells and zebrafish embryos to demonstrate their great biocompatibility. By taking advantage of their extreme brightness and minimal cytotoxicity, we performed, for the first time, in vivo microangiography imaging on living zebrafish embryos using Pdots. These quinoxaline-based NIR-fluorescent Pdots are anticipated to find broad use in a variety of in vitro and in vivo biological research.

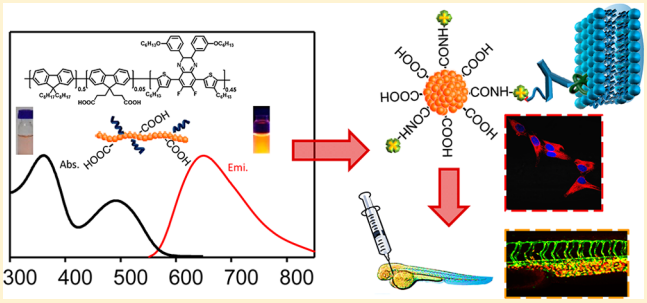

INTRODUCTION

There have been considerable efforts in the development of optical imaging techniques with fluorescence microscopy due to their high signal-to-noise ratio, excellent spatial and/or temporal resolution, and noninvasive nature, rendering them extremely useful in the investigation of biological processes in live organisms. In recent years, the development of several super-resolution fluorescence microscopy techniques has successfully surpassed the diffraction limit of light and these technologies have been employed to visualize biological structures with a spatial resolution of 10−30 nm.[1−9] Moreover, the new breakthroughs in fluorescence image-guided surgery[10,11] and its first in-human proof-of-concept staging and debulking surgery for ovarian cancer[12,13] have also strongly highlighted the importance of choosing a photostable, biocompatible, bright, and tumor-specific fluorescent agent. In the past few years, intraoperative imaging by use of visible to invisible near-infrared (NIR) fluorescent light has played an important role between the gap of preoperative detection and intraoperative techniques. Particularly for the contrast agents with emission in the NIR range (700−1400 nm), they have been widely exploited in bioimaging and clinical diagnosis. It is because NIR light can travel several millimeters (up to centimeters) through blood or tissues, and minimal scattering or autofluorescence of biological species is observed in the NIR spectrum.[14,15] Among these NIR contrast agents for intraoperative imaging, only a paucity of fluorophores (e.g., indocyanine green and methylene blue) have been approved for clinical or preclinical trial.[13]

As compared to conventional organic dyes, nanoparticle-based imaging agents (e.g., dye-doped silica/polymeric nanoparticles[16−20] or quantum dots[21−23]) exhibit much higher brightness and thereby can be used to improve the temporal resolution in bioimaging. Nevertheless, several concerns such as leakage of the doped dyes from the silica/polymeric matrix[24,25] and the potential release of the toxic inorganic compounds (e.g., cadmium)[26−28] might largely restrict their biological use and clinical implementation.

Very recently, semiconducting polymer nanoparticles (Pdots) have emerged as a new type of highly fluorescent probes that possess extraordinary fluorescence brightness, superior photostability, high emission rates, and minimal toxicity to cells and tissues.[29−47] More importantly, Pdot-based NIR fluorescent agents offer significant advantages over conventional small fluorophores because most NIR fluorescent dyes are subjected to poor solubility in aqueous solutions, fast photobleaching, low fluorescence brightness, and small Stokes shift. Although great efforts have been exerted to develop NIR fluorescent Pdots, various challenges have impeded the

Received: June 29, 2015
Published: August 10, 2015

DOI: 10.1021/jacs.5b06710
J. Am. Chem. Soc. 2015, 137, 10420−10429

progress, especially for the severe aggregation-caused emission quenching of the rigid and flat $\pi-\pi$ stacking of the conjugated scaffolds of NIR-emitting polymers upon condensation into a Pdot form. Several strategies have been explored to tackle this self-quenching problem. One approach is to encapsulate NIR dyes or polymers into the Pdot matrix, resulting in efficient energy transfer from Pdot to the doped dyes or polymers.[48−50] However, the leakage of the dopant molecules from the Pdot matrix remains a serious issue in many applications that require long-term monitoring.[51] To address the leaking issue, our group have successfully developed a facile method by capping the dye-embedded Pdots with polydiacetylenes.[52−54] Another strategy is the direct synthesis of NIR-emitting polymers by incorporating NIR-fluorescing chromophores into the semiconducting polymer backbone. To date, however, only a very small molar fraction of NIR chromophores (usually <3%) could be incorporated into the Pdot matrix due to the important issue of self-quenching at higher molar concentrations.[55,56] Very recently, we have designed and synthesized a series of dithienylbenzoselenadiazole (DBS)-based copolymers to form NIR fluorescent Pdots where ∼10% of DBS units could be incorporated once the alkyl substitution was introduced onto the DBS monomer to alleviate self-quenching phenomenon.[57] However, the relatively low molar percentage of NIR emitters inside the polymer could cause diminished photostability of the resulting Pdots if a stronger laser excitation is used for prolonged periods of time.[57] Besides, this type of Pdots is unable to provide high brightness once excited at the absorption maximum of the NIR monomers owing to their low absorption.

To address the above-mentioned challenges, we here describe the design and synthesis of quinoxaline-based Pdots that show bright NIR emissions and can be readily excited by a conventional 488- or 532 nm laser. More importantly, the molar fraction of NIR chromophores (i.e., quinoxaline) incorporated inside the semiconducting polymers can be as high as 50% with a quantum yield up to 47%. Additionally, we directly functionalized carboxyl groups on the side chains of the polymers for further biomolecular conjugation and specific cellular labeling. Single-particle brightness analysis reveals that the per-particle brightness of the quinoxaline-based Pdots is about 6-8 times brighter than that of quantum dots. We also performed in vivo microangiography imaging on living zebrafish. The high quantum yield, large absorption cross-section in the visible region, and large Stokes shifts of these quinoxaline-based Pdots are promising in a broad range of in vitro/vivo bioimaging and analytical detection.

RESULTS AND DISCUSSION

Our aim was to synthesize quinoxaline-based Pdots with ultrabright red to NIR emission and investigate how the long alkyl chains on the thiophene rings as well as the fluorine atoms on the quinoxaline moieties affect their optical properties. We further functionalized the polymers with carboxylate groups for in vitro specific cellular labeling and in vivo biological imaging.

Design and Synthesis of Quinoxaline-Containing Copolymers with NIR Fluorescence. In an effort to develop NIR fluorescent semiconducting polymers, we exploited the donor−acceptor concept in which strong electron-donating units and strong electron-accepting moieties (i.e., NIR-emitting units) were integrated into the polymer backbone to synthesize the low bandgap copolymers. Unfortunately, the serious aggregation-induced fluorescence quenching of the flat and rigid NIR-emitting derivatives usually results in the fact that the fluorescence quantum yields of the polymers decrease dramatically with increasing concentrations of NIR units. As a trade-off, therefore, only a small molar ratio (∼3%) of NIR chromophores can be incorporated into the polymers in order to obtain a high quantum yield. Because the fluorescence brightness is calculated from the product of the peak absorption cross-section and the fluorescence quantum yield, the low molar concentration of NIR chromophores would cause low fluorescence brightness if the polymer was excited at the absorption peak of the NIR monomers. As such, the polymers can be excited only at the absorption of the energy donor (i.e., fluorene, λ_{max}^{abs} < 400 nm). Here we intend to circumvent this issue by the employment of bulky quinoxaline monomers with various substituents because we expect the steric hindrance from the fairly large quinoxaline derivatives can efficiently eliminate the phenomenon of aggregation-caused quenching. Specifically, we first synthesized a series of quinoxaline-based monomers and then polymerized with fluorene via palladium-catalyzed Suzuki coupling to form a series of copolymers a shown in Figure 1. Here we fixed the molar percentage of

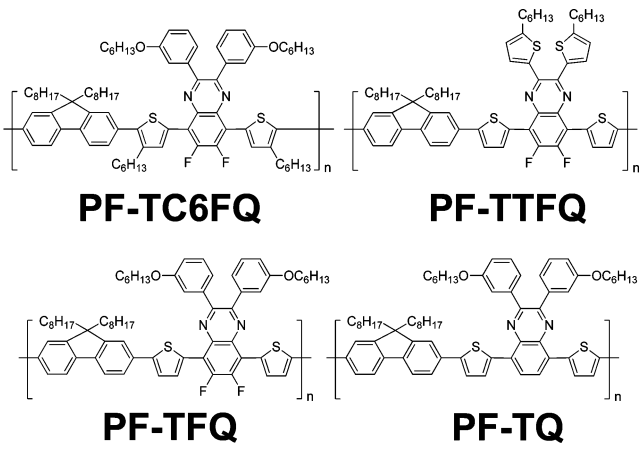

Figure 1. Chemical structures of a series of quinoxaline-containing polymers.

quinoxaline emitters at 50% so that the resulting copolymers can be directly excited at the quinoxaline monomers (λ_{max}^{abs} = 450−600 nm, vide infra), which is more favorable for many biological applications.

The general synthetic routes for the monomers and polymers were illustrated in Scheme 1. Compound **2** and **6** were synthesized according to previously reported literatures with modified procedures.[58−60] Fluorinated compound **8** was then synthesized by reacting compound **2** with **6**. Monomer **10** was obtained by use of Stille coupling from compound **7** and **8**, followed the bromination using NBS. Monomers **11**−**13** were synthesized according to the reported literature with modified procedures (see Supporting Information).[58,61,62] Finally, Suzuki polymerization between fluorene derivative **14** and monomers **10**, **11**, **12**, and **13** with $Pd(PPh_3)_4$ catalyst gave quinoxaline-containing conjugated copolymers **PF-TC6FQ**, **PF-TTFQ**, **PF-TFQ**, and **PF-TQ**, respectively. We also directly functionalized the conjugated copolymers with carboxylate groups on the substituents of polyfluorene to prevent the leaking problem which is frequently confronted by other functionalization approaches such as surface encapsulation or polymer coprecipitation startegies.[51] For instance, we incorporated

DOI: 10.1021/jacs.5b06710
J. Am. Chem. Soc. 2015, 137, 10420−10429

Scheme 1. Synthetic Routes of Quinoxaline Comonomers and Copolymers

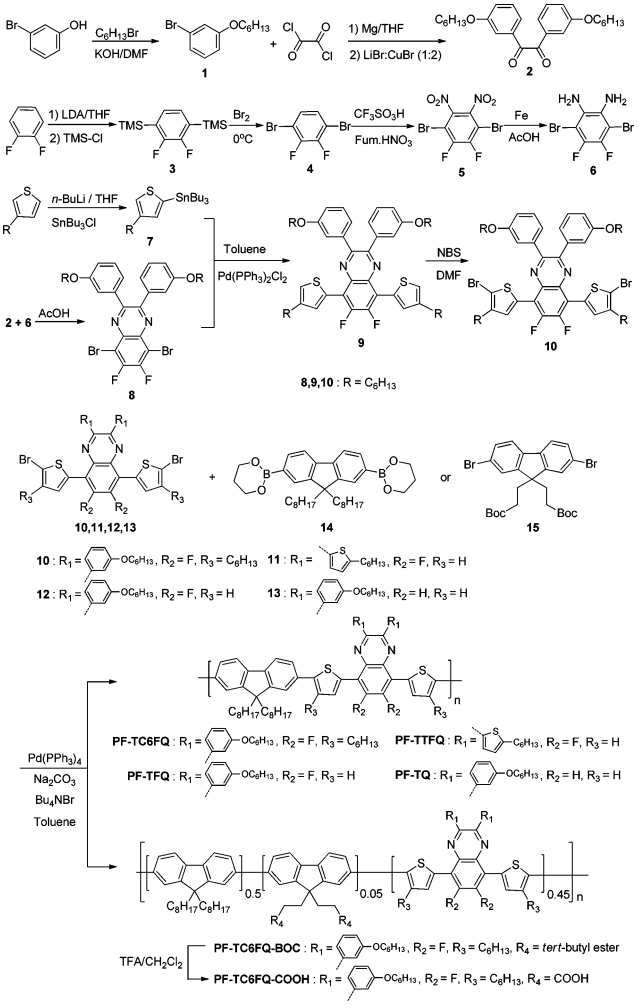

Scheme 2. (A) Preparation of Carboxyl-Functionalized Quinoxaline-Based Pdots and Subsequent Bioconjugation for Specific Celluar Labeling;[a] (B) Hydrodynamic Diameter of PF-TC6FQ-COOH Pdots Measured by Dynamic Light Scattering (Left) and their Corresponding Transmission Electron Microscopy Images (Right);[b] (C) Gel Electrophoresis of Bare Pdots, Streptavidin-Conjugated Pdots, and Folate-Functionalized Pdots

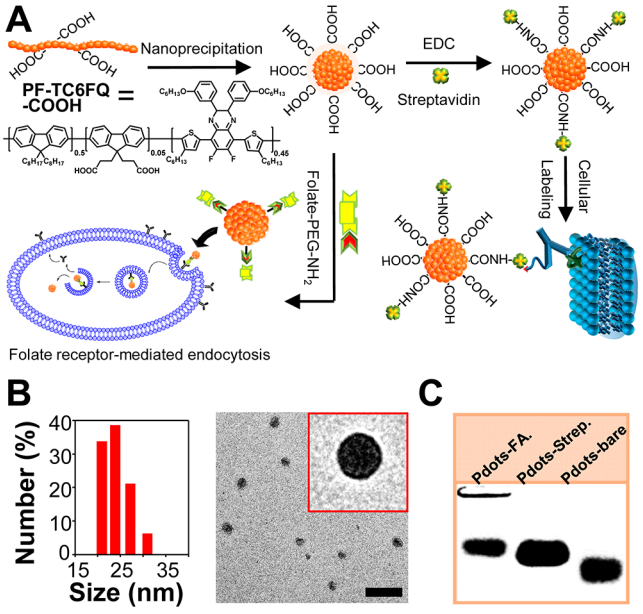

[a]The conjugated polymer (**PF-TC6FQ-COOH** as an example in this scheme) was dissolved in THF and then nanoprecipitated in water under vigorous sonication to form Pdots. The carboxylic-acid-functionalized Pdots were then conjugated to streptavidin or folic acid through EDC-catalyzed coupling for specific cellular targeting. [b]Scale bar is 100 nm.

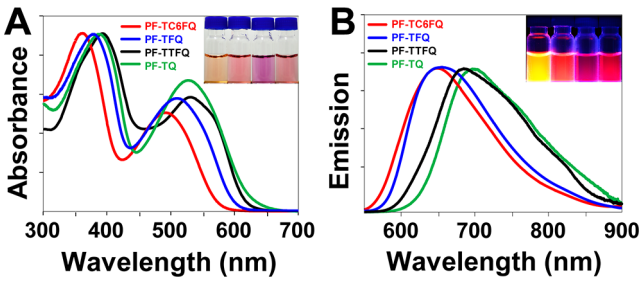

Figure 2. (A) Absorption spectra of **PF-TC6FQ**, **PF-TFQ**, **PF-TTFQ**, **PF-TQ** Pdots series in water. The inset shows the photograph of the Pdot solutions (from left to right: **PF-TC6FQ**, **PF-TFQ**, **PF-TTFQ**, and **PF-TQ** Pdots). (B) Emission spectra of **PF-TC6FQ**, **PF-TFQ**, **PF-TTFQ**, **PF-TQ** Pdots series in water. The inset shows the photograph of the Pdot solutions under 365 nm UV light illumination (from left to right: **PF-TC6FQ**, **PF-TFQ**, **PF-TTFQ**, and **PF-TQ** Pdots).

compound **15**, a carboxyl-functionalized fluorene moiety, into the conjugated backbone of **PF-TC6FQ-BOC** polymer and then removed the protection group (*tert*-butyl) by using trifluoroacetic acid to obtain **PF-TC6FQ-COOH** (Scheme 1). It is worth mentioning that we integrated only 5% carboxyl groups within the polymer backbone because Chiu's group has demonstrated that the incorporation of carboxyl groups with a low density can form stable and bright Pdots without nonspecific adsorption toward biomolecules.[63] The carboxylate functional polymers (e.g., **PF-TC6FQ-COOH**) can thereby be conjugated with biomolecules for biological applications.

Photophysical Properties of Quinoxaline-Based Pdots. The preparation of Pdots and the subsequent surface functionalization was illustrated in Scheme 2A. The average diameter of Pdots determined by dynamic light scattering (DLS) and transmission electron microscopy (TEM) was 22 nm (Scheme 2B). Scheme 2C show the result of gel electrophoresis in which bare **PF-TC6FQ-COOH** Pdots moved faster than both streptavidin-modified and folate-functionalized Pdots. This result can be ascribed to the reduced negative charged on the Pdot surfaces because of the consumption of the carboxyl groups after streptavidin or folate conjugation. The absorption and emission spectra of four different types of quinoxaline-containing Pdots are shown in Figure 2. The absorption peaks at 350−430 nm and 450−600 nm are attributed to polyfluorene segments and quinoxaline units, respectively. The insets in Figure 2A and 2B represent the photographs of Pdot solutions under white light and 365 nm UV light, respectively (from left to right: **PF-TC6FQ**, **PF-TFQ**, **PF-TTFQ**, and **PF-TQ** Pdots). We found that the introduction of thiophene moieties on the quinoxaline monomer (**PF-TFQ** vs **PF-TTFQ**) led to the redshift of both the absorption and emission spectra because of the

DOI: 10.1021/jacs.5b06710
J. Am. Chem. Soc. 2015, 137, 10420−10429

increased conjugation system. On the other hand, the incorporation of two electron-withdrawing fluorine atoms blueshifted the absorption and fluorescence peaks (**PF-TFQ** vs **PF-TQ**), probably due to the enhanced charge transfer inside the polymer backbone.[64,65] Moreover, the alkyl substitution on the thiophene rings slightly blueshifted the absorption and fluorescence peaks (**PF-TC6FQ** vs **PF-TFQ**) owing to the reduced conjugation length caused by kinking or bending of the polymer chain. Their photophysical properties in Pdot form were summarized in Table 1.

Table 1. Summary of Optical Properties of Quinoxaline-Based Copolymer Series in Pdot Form in Water

copolymers	λ_{max}^{abs} (nm)[a]	λ_{max}^{em} (nm)[b]	size (nm)	Φ (%)[c]	τ (ns)[d]
PF-TC6FQ	362, 493	652	21	47	1.46
PF-TFQ	379, 511	664	23	11	0.68
PF-TTFQ	392, 531	695	28	8	0.89
PF-TQ	389, 529	712	27	9	1.08

[a]Absorption maximum. [b]Fluorescence maximum. [c]Quantum yield. [d]Fluorescence lifetime.

The quantum yields of **PF-TC6FQ**, **PF-TFQ**, **PF-TTFQ**, and **PF-TQ** in aqueous solutions were determined to be 47, 11, 9, and 8%, respectively. It can be clearly observed that the incorporation of thiophene moieties on the quinoxaline monomer (**PF-TFQ** vs **PF-TTFQ**) eliminated the fluorescence quantum yield (11 to 9%) although both the absorption and the emission maxima were modestly red-shifted (20−30 nm). However, the introduction of fluorine atoms (**PF-TFQ** vs **PF-TQ**) only slightly raised the quantum yield. Most importantly, the integration of the hexyl alkyl chains into the thiophene rings (e.g., **PF-TC6FQ**) drastically increased the quantum yield (11 to 47%), suggesting that the extent of aggregation-cased quenching was effectively prohibited. It should be noted that the molar percentage of quinoxaline for all copolymers was fixed at 50%, indicating that the resulting Pdots could be directly excited by a commonly used 488 or 532 nm laser rather than a 405 nm laser to facilitate energy from polyfluorene to quinoxaline.

Additionally, we used a time-correlated single-photon counting module system to determine the fluorescence lifetime (τ) of this series of quinoxaline-based Pdots (Figure S1). The fluorescence radiative decay rate constant (K_R) and non-radiative rate constant (K_{NR}) containing all possible non-radiative decay pathways can also be estimated from the combination of the following two equations:

$$\Phi = K_R/(K_R + K_{NR}) \quad (1)$$

$$\tau = (K_R + K_{NR})^{-1} \quad (2)$$

Take **PF-TC6FQ** Pdots as an example, the **PF-TC6FQ** Pdots have a fluorescence radiative decay rate of 3.2×10^8 s^{-1}, which is comparable to other types of Pdots.[44,52,56]

Single-Particle Fluorescence Brightness Comparison. As a new type of fluorescent probe, single-particle brightness is one of the important properties for Pdots to be evaluated.[66] The fluorescence brightness can be estimated by the product of peak absorption cross section and the fluorescence quantum yield, in which the absorption cross-section refers to the light-harvesting ability. Table 2 summarizes the optical properties of quinoxaline-containing Pdot aqueous solutions in comparison to several NIR dyes and quantum dots. Here we take **PF-TC6FQ** as an example because of its high quantum yield. The per-particle absorption cross sections (σ) of the Pdots were obtained from the analysis of the UV−visible absorbance at known Pdot concentrations (Beer's Law) and the absolute quantum yields (Φ) were measured by use of an integrating sphere unit. For example, the per-particle absorption cross-section of **PF-TC6FQ** Pdots (21 nm) at 493 nm was determined to be 2.00×10^{-13} cm^2. Because the final brightness of Pdots is the product of the absorption cross-section and the fluorescence quantum yield, the brightness of **PF-TC6FQ** Pdots was calculated to be 9.20×10^{-13} as shown in Table 2. The results show that **PF-TC6FQ** Pdots possess the highest fluorescence brightness, which is around 3 orders of magnitude higher than conventional organic dyes or 3−5 times brighter than that of Qdots655 and Qdots705 quantum dots (purchased from Invitrogen), when excited at their absorption maxima. Additionally, we found that **PF-TC6FQ** Pdots are calculated to be ∼8 times brighter than Qdots655/Qdots705 nanocrystals under 488 nm laser excitation (values are shown in the brackets in Table 2). We further performed single-particle imaging to experimentally compare the single-particle brightness between **PF-TC6FQ** Pdots and Qdots655 under identical excitation (488 nm) and acquisition conditions. As shown in Figure 3 where the intensity histograms were collected by analyzing hundreds of nanoparticles for each samples, we found that the average per-particle brightness of **PF-TC6FQ** Pdots were 6−7 times higher than that of Qdots655, consistent with the calculated results. The photostability of Pdots were also evaluated as compared to Cy5.5 and it can be clearly observed that Pdots appeared to be extraordinarily photostable (Figure S2).

Bioconjugation and Specific Cellular Labeling with PF-TC6FQ-COOH Pdots. We next employed these quinoxaline-based Pdots for both cell-surface and subcellular labeling to demonstrate their potential in biological applications. In one experiment, subcellular microtubule labeling inside HeLa cells

Table 2. Photophysical Data of Quinoxaline-Based Pdots in Water Compared with Other Water-Soluble Typical NIR Dyes

fluorescent probes	λ_{max}^{abs} (nm)	λ_{max}^{em} (nm)	fwhm[e] (nm)	ε_{max} (M^{-1} cm^{-1})	σ (cm^2)	size (nm)	Φ (%)	brightness (σ × Φ) (cm^2)
ATTO740[a]	740	764	43	1.20×10^5	4.58×10^{-16}	–	10	4.58×10^{-15}
Cy 5.5[b]	674	694	44	1.95×10^5	7.45×10^{-16}	–	23	1.71×10^{-14}
NIR7.0−2[b]	777	798	50	1.20×10^5	4.58×10^{-16}	–	2.5	1.15×10^{-15}
Qdots655[c]	405 (488)	651	30	$5.70\ (2.90) \times 10^6$	$2.18\ (1.11) \times 10^{-14}$	11	91	$1.98\ (1.01) \times 10^{-12}$
Qdots705[c]	405 (488)	705	66	$8.30\ (3.00) \times 10^6$	$3.17\ (1.15) \times 10^{-14}$	14	82	$2.60\ (0.94) \times 10^{-12}$
PF-TC6FQ[d]	493 (488)	652	129	$5.23\ (5.20) \times 10^7$	$2.00\ (1.99) \times 10^{-13}$	21	46	$9.20\ (9.15) \times 10^{-12}$
PF-TQ[d]	529	712	148	1.32×10^8	5.04×10^{-13}	27	9	4.54×10^{-12}

[a]Data from ATTO-TEC catalog. [b]Data from ref 73. [c]Data from Invitrogen (Life Technologies). [d]Pdots in deionized water. [e]Full width at half-maximum.

DOI: 10.1021/jacs.5b06710
J. Am. Chem. Soc. 2015, 137, 10420−10429

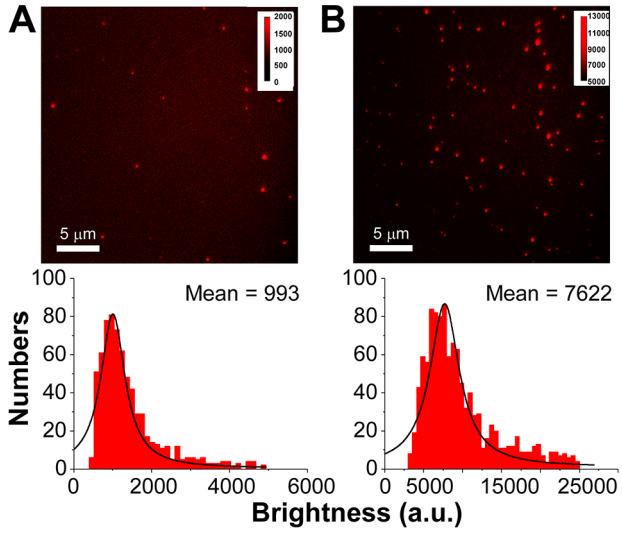

Figure 3. (A) Single-particle fluorescence image of commercial Qdots655 (upper graph) and the corresponding histograms showing the intensity distributions (bottom graph). (B) Single-particle fluorescence image of **PF-TC6FQ** Pdots (upper graph) and the corresponding histograms showing the intensity distributions (bottom graph). The black curves were obtained by fitting a log-normal distribution to the histogram, resulting in mean brightness of 993 and 7622 counts for Qdots655 and **PF-TC6FQ** Pdots, respectively. Both images were obtained with a 488 nm laser under the same excitation power and identical detection conditions.

was performed. We first conjugated streptavidin onto the surface of Pdots via 1-ethyl-3-[3-(dimethylamino)propyl]-carbodiimide hydrochloride-(EDC)-catalyzed coupling (Scheme 2A). We then incubated Pdot-streptavidin conjugates together with biotinylated monoclonal anti-α-tubulin antibody with HeLa cells so that Pdots could label the microtubules of HeLa cells. Figure 4A–C shows representative confocal images of Pdot labeled microtubules in HeLa cells, indicating Pdots could be specifically targeted onto subcellular structures in the presence of biotinylated antibody. No noticeable fluorescence

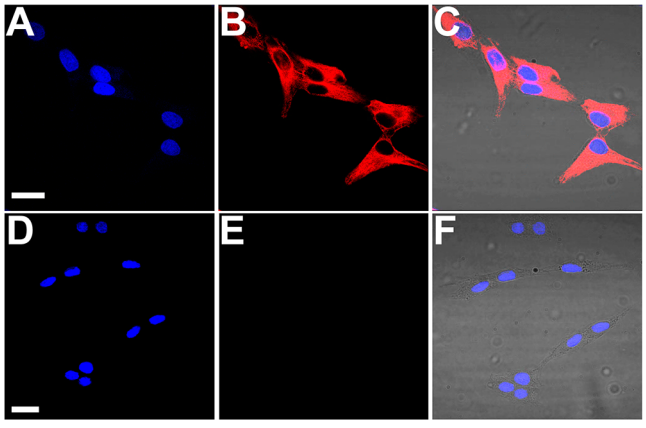

Figure 4. Two-color confocal microscopy images of microtubules in HeLa cells labeled with Pdot-streptavidin conjugates. The blue fluorescence was from nuclear counterstain Hoechst 34580 and the red fluorescence was from Pdot-streptavidin. (A) Image of nucleus. (B) Image of microtubules. (C) The overlay of panels (A) and (B). (D–F) Images of negative control samples where cells were incubated with Pdot-streptavidin conjugates but in the absence of biotinylated primary antibody. The scale bars are 30 μm.

signal from Pdots was observed for negative control samples (Figure 4D–F) where the experimental conditions were identical as that in Figure 4A–C except for the absence of the biotinylated primary antibody. These results indicate this new class of quinoxaline-based Pdots exhibit highly specific binding activity with minimal nonspecific adsorption. The cellular labeling of **PF-TQ** Pdots was also performed (Figure S3).

In addition to the above-mentioned specific labeling through the strong and stable streptavidin–biotin interaction, we also utilized receptor-mediated endocytosis, a commonly used strategy for in vivo tumor targeting, to label cancer cells. Here we functionalized the surface of Pdots with folic acid and then incubated with SKOV-3 cancer cells with overexpressed folate receptors. As shown in Figure 5A, red fluorescence was

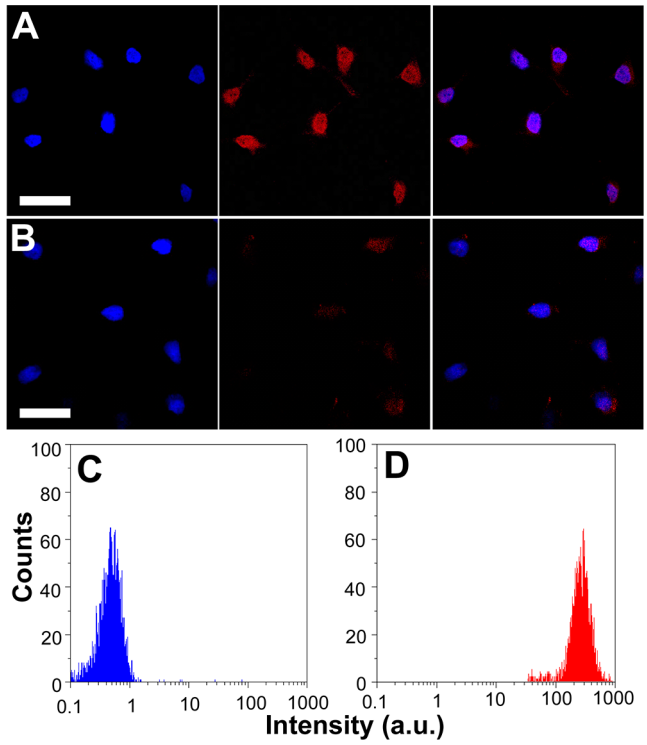

Figure 5. Confocal fluorescence images of SKOV-3 cells labeled by Pdot-folate conjugates and the flow cytometry results using MCF-7 cells. (A) Blue fluorescence is from nuclear counterstain Hoechst 34580, and red fluorescence is from Pdot-folate conjugates. The right panel shows fluorescence overlaid of blue and red fluorescence. (B) Images of negative control samples in which cells were incubated with bare Pdots without folate functionalization. The scale bars are 30 μm. (C) Flow cytometry measurements of MCF-7 breast cancer cells labeled by Pdot-streptavidin conjugates via nonspecific binding (negative control, no primary biotin antihuman CD326 EpCAM antibody). (D) Fluorescence intensity distribution of MCF-7 cells labeled via positive specific targeting using Pdot-streptavidin conjugates.

clearly observed for Pdot-folate stained SKOV-3 cells, while a significantly lower red fluorescence signal was found for bare Pdot (without folate functionalization) treated cells (Figure 5B). The results reveal that folate-functionalized Pdots could be internalized into SKOV-3 ovarian cancer cells via folate receptor-mediated endocytosis pathways. We believe this strategy could be further expanded for in vivo studies on tumor-bearing mice models if needed.

DOI: 10.1021/jacs.5b06710
J. Am. Chem. Soc. 2015, 137, 10420–10429

Moreover, we also executed flow cytometry experiments using Pdot-streptavidin to label membrane proteins on MCF-7 cells. Here, the Pdot-streptavidin conjugates, together with primary biotin antihuman CD326 EpCAM antibody were labeled onto the surfaces of live MCF-7 cells. The quinoxaline-based Pdots exhibit emissions in the NIR, which is beneficial in many biological studies. Figure 5C−D shows the flow cytometry results in which an excellent separation between Pdot-targeted cells (Figure 5D, with primary antibody) and the negative control/background (Figure 5C, without primary antibody). These results demonstrate Pdots could be targeted to MCF-7 cells effectively and specifically with minimal nonspecific binding, consistent with the results from confocal microscopy in HeLa cells. Their corresponding confocal microscopy images were also shown in Figure S4.

In Vivo Cytotoxicity and Microangiography Imaging in Zebrafish. For biological applications and translation of these NIR fluorescent Pdots, the cytotoxicity of Pdots is the major concern. We first conducted ex vivo cytotoxicity experiments using MTT assay and found minimal cytotoxic effect of these Pdots (10 nM) on HeLa cells. (Figure S5). Additionally, we assessed in vivo toxicity by using zebrafish model as shown in Figure 6A in which the results demonstrate that the zebrafish could grow normally in the presence of Pdots (2−4 nM). Both ex vivo and in vivo results suggest that these Pdots exhibit high biocompatibility and should be suitable for advanced biological applications. For in vivo biological applications, zebrafish present an excellent animal model for several reasons, which can accelerate our understanding in nanoparticle toxicity and bioimaging.[67] For example, zebrafish are evolutionarily close to human and can produce more than 100 embryos in a single mating. Besides, zebrafish embryos are optically transparent and can be genetically modified which allow for the direct observation of biological behaviors. For in vivo microangiography imaging on zebrafish, we injected **PF-TC6FQ-COOH** Pdots into the sinus venosus of the embroys. As shown in Figure 6B(a−c), we found that the Pdots (red fluorescence) were immediately carried away with the blood-stream and distributed in all the vascular system. Figure 6B(d−f) show representative images of Pdot microangiography in zebrafish larvae. The blood vessel walls which consisted of eGFP-expressing endothelial cells exhibited green fluorescence, while the lumen of the vessels displayed red fluorescence of Pdots. Although some Pdots inevitably deposited on the endothelial walls probably due to the hydrophilicity of Pdot surface, Pdots remained stable in the blood circulation without observation of leaking even 2 h after injection. In vivo microangiography imaging on zebrafish using **PF-TQ** Pdots was also shown in Figure S6. These Pdots show high fluorescence brightness and good biocompatibility, which might be used for further in vivo targeting[37] and long-term observation or tracking.[20,68−70]

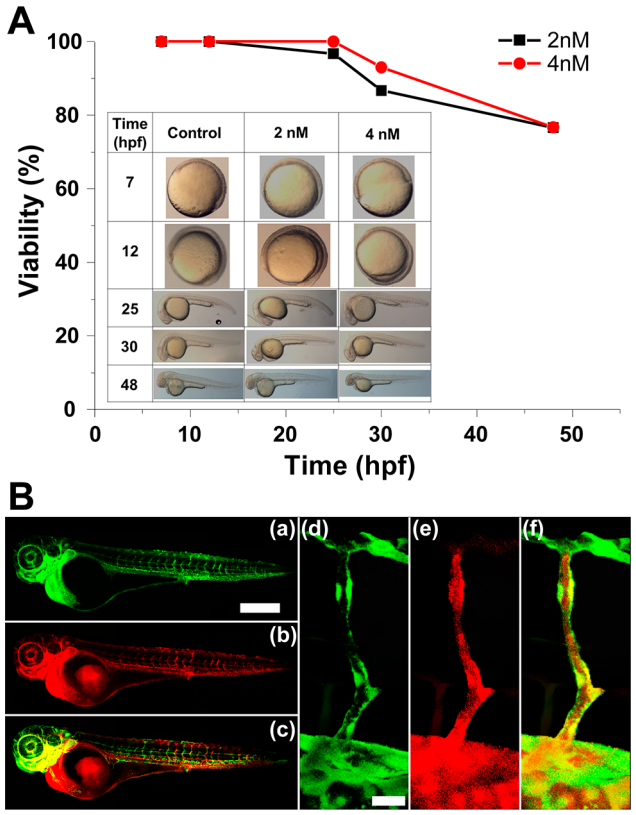

Figure 6. (A) Biotoxicity assessment of Pdots by zebrafish model. Time course recording morphology of zebrafish embryos exposed to 2 and 4 nM Pdot solutions in the period of 0−48 h post fertilization (hpf). (B) Zebrafish microangiography by injection of **PF-TC6FQ-COOH** Pdots into 3 days post fertilization *Tg(kdrl:eGFP)* zebrafish embryos. The global view of zebrafish vessels and Pdots images is shown in left panels (a−c), while a close view of the trunk vasculature (intersegmental vessel, ISV) is shown in the right panels (d−f). Green emission is from endothelial cells expressing eGFP and red emission is from Pdots. Scale bars represent 400 μm in a−c and 20 μm in d−f, respectively.

CONCLUSIONS

In summary, we have successfully developed a series of ultrabright NIR-emitting Pdots with large Stokes shifts based on quinoxaline derivatives. We also found the alkyl substitution and fluorine atom on thiophene rings in quinoxaline plays an important role in the interchain interaction at an increased quinoxaline concentration. These Pdots can be readily excited by a 488 nm laser or a longer wavelength (e.g., 532 nm) laser due to the high molar percentage (i.e., 50%) of quinoxaline emitters inside the polymer backbones. Single-particle brightness measurements indicate that the quinoxaline-based Pdots can be up to 8 times brighter than Qdots655. Besides, the covalent fabrication of carboxylic acid groups on the side chains of fluorene monomers offered the feasibility for further conjugation and analytical detection. We have demonstrated the bioconjugation of the carboxyl-functionalized Pdots and their highly specific binding to both cell surfaces and interiors without any detectable nonspecific binding. We also performed in vivo microangiography imaging on zebrafish. We anticipate this new type of quinoxaline-based NIR-emitting Pdots to find broad use both in basic biological studies and in bioimaging and bioanalytical applications.

EXPERIMENTAL SECTION

Materials. All of the chemicals were purchased from Sigma-Aldrich or Alfa Aesar, and used as received unless indicated elsewhere. All biorelated agents such as streptavidin, anitibody, or medium are purchased form Invitrogen (Life Technologies). High purity water (18.2 MΩ·cm) was used throughout the experiment. All ^{1}HNMR and ^{13}CNMR spectra were recorded on a Bruker AV300 spectrometer (300 MHz).

Synthesis of 1-Bromo-3-hexyloxybenzene, 1..[59−61] Potassium carbonate (3.75 g, 66.8 mmol) was added to the solution of 3-

DOI: 10.1021/jacs.5b06710
J. Am. Chem. Soc. 2015, 137, 10420−10429

bromophenol (5 g, 28.9 mmol) and 1-bromohexane (7.14 g, 43.3 mmol) in dimethyl foramide (DMF, 50 mL), and the reaction mixtures were stirred at 90 °C under nitrogen atmosphere overnight. After that, the solid was filtered out and the solvent was removed by a rotary evaporator. The crude product was purified by column chromatography on silica gel using hexane as eluent to afford 3.7 g (50%) of compound **1** as colorless liquid. ^{1}H NMR (300 MHz, $CDCl_3$) δ 7.10 (t, J = 8.4 Hz, 1H), 7.05−7.02 (m, 2H), 6.81−6.78 (m,1H), 3.90 (t, J = 6.4 Hz, 2H), 1.75 (m, J = 6.8 Hz, 2H), 1.46−1.39 (m, 2H), 1.36−1.26 (m, 4H), 0.89 (t, J = 6.8 Hz, 3H).^{13}C NMR (75 MHz, $CDCl_3$) δ 159.93, 130.40, 123.47, 122.73, 117.69, 113.49, 68.69, 31.51, 29.07, 25.63, 22.56, 13.98. HRMS (ESI) (M^+, $C_{12}H_{17}BrO$) calcd 256.0463, found 256.0460.

Synthesis of 1,2-Bis(3-hexyloxyphenyl)ethane-1,2-dione, 2..[59−61] A solution of 1-Bromo-3-hexyloxybenzene, labeled as Solution A, was prepared as follows: 5 mL of 2.5 M *n*-butyllithium (12.5 mmol) in hexanes was added via cannula to 20 mL of anhydrous THF, previously cooled to −78 °C under nitrogen atmosphere. The mixture was stirred for 10 min, and then 1.17 mL of 1-Bromo-3-hexyloxybenzene (2.04 g, 12.5 mmol) was added dropwise. The mixture was stirred for 150 min, and the temperature was kept at −78 °C. Meanwhile, a solution, labeled as Solution B, was prepared as follows: In a 250 mL round-bottom flask (equipped with stir bar and a septum), containing 50 mL of anhydrous THF, was added LiBr (1.09 g, 12.5 mmol, 1 equiv) and CuBr (1.79 g, 12.5 mmol, 1 equiv), the CuBr and LiBr mixture was stirred until all the salts were dissolved. The mixture was then cooled to −40 °C or to lower temperatures. Solution C: 483 μL of oxalyl chloride (714 mg, 5.63 mmol, 0.45 equiv) was dissolved in 10 mL of anhydrous THF in a 100 mL round-bottom flask (previously equipped with a septum) and then cooled to −40 °C or to lower temperatures. Solution A was added via cannula to Solution B, and the mixture was stirred for 5 min. Finally Solution C was slowly added to the mixture via cannula. The mixture was kept in a cold bath for 2 h, allowed to warm up to room temperature. After that, the reaction was quenched with 100 mL of saturated NH_4Cl aqueous solution and then extracted with ethyl acetate, and dried over anhydrous $MgSO_4$. The solvent was removed via rotary evaporation, and was subsequently purified by column chromatography on silica gel by using ethyl acetate/hexane (1:7, v/v) as eluent to afford 1.1 g (34%) of compound **2** as yellow liquid. ^{1}H NMR (300 MHz, $CDCl_3$) δ 7.49 (m, 2H), 7.43 (m, 2H), 7.35 (t, J = 10.4 Hz, 2H), 7.18−7.15 (m, 2H), 3.98 (t, J = 6.4 Hz, 4H), 1.77 (m, 4H), 1.47−1.40 (m, 4H), 1.34−1.29 (m, 8H), 0.88 (t, J = 7.2 Hz, 6H). ^{13}C NMR (75 MHz, $CDCl_3$) δ 194.52, 159.62, 134.21, 129.95, 122.91, 122.19, 113.62, 68.35, 31.51, 29.05, 25.63, 22.55, 13.98. HRMS (ESI) (M^+, $C_{26}H_{34}O_4$) calcd 410.2457, found 410.2462.

Synthesis of 2,3-Difluoro-1,4-bis(trimethylsilyl)benzene, 3. 5.7 mL (40.3 mmol) of *n*-butyllithium (1.6 M in exane) was added to a solution of diisopropylamine (5.7 mL, 40.3 mmol) in anhydrous THF (20 mL) at 78 °C under nitrogen atmosphere. After being stirred at 78 °C for 30 min, 1,2-difluorobenzene (1.7 mL, 17.5 mmol) and chlorotrimethylsilane (4.9 mL, 38.5 mmol) was added to the solution at a rate which allowed the internal reaction temperature to remain below 50 °C. The solution was stirred at −78 °C for additional 1 h and then 1 M H_2SO_4 solution (10 mL) was added to extract with diethyl ether for three times. The combined organic layers were washed with brine, dried over $MgSO_4$, and concentrated under reduced pressure to afford 3.5 g (77%) of compound **3** as colorless needle-shaped crystals. ^{1}H NMR (300 MHz, $CDCl_3$) δ 7.09 (s, 2H), 0.32 (s, 18H). HRMS (ESI) (M^+, $C_{12}H_{20}F_2Si_2$) calcd 258.1072, found 258.1071.

Synthesis of 2,3-Difluoro-1,4-dibromobenzene, 4. To a one-bottomed flask was added 2.3 mL (43.8 mmol) of bromine and then cooled to 0 °C. 3.5 g (13.5 mmol) of compound **3** was added portionwise while maintaining the internal temperature at 20 to 40 °C. The reaction mixture was stirred at 60 °C for 1 h and then additional 0.4 mL (7.30 mmol) of bromine was added to stir for another 1h. The reaction mixture was cooled to 0 °C and slowly poured into ice-cold saturated $NaHCO_3$ solution to extract with diethyl ether. The organic layer was washed with brine, dried over $MgSO_4$, and concentrated under reduced pressure to afford 3.2 g (87%) of compound **4** as yellow liquid. ^{1}H NMR (300 MHz, $CDCl_3$) δ 7.23 (m, 2H). HRMS (ESI) (M^+, $C_6H_2Br_2F_2$) calcd 269.8491, found 269.8488.

Synthesis of 1,4-Dibromo-2,3-difluoro-5,6-dinitrobenzene, 5..[59−61] 5 mL of fuming nitric acid was added dropwise to trifluoromethanesulfonic acid (100 mL) in an ice bath and stirred for 30 min. 3.2 g (11.77 mmol) of compound **4** was added to the mixture in portions over 30 min. After stirring at room temperature for 2 h, the mixture was cooled down to 0 °C and then another 5 mL of fuming nitric acid was added slowly to react overnight at 70 °C. After that, the reaction mixture was poured into cold water. The precipitate was filtered and then recrystallized from ethanol to yield 2.5 g (59%) of compound **5** as a yellow solid. HRMS (ESI) (M^+, $C_6Br_2F_2N_2O_4$) calcd 359.8193, found 359.8196.

Synthesis of 1,4-dibromo-2,3-difluoro-5,6-diaminobenzene, 6..[59−61] To a one-bottomed flask was added 0.35 g (0.97 mmol) of compound **5**, 0.40 g (7.1 mmol) of iron powder, and 12 mL of acetic acid. The reaction mixture was stirred at 45 °C for 4 h before poured into 25 mL of cold 5% NaOH solution. The solution was extracted with ether and then the organic phase was washed with 5% $NaHCO_3$ solution for 5 times. After dried over $MgSO_4$, the solvent was removed under reduced pressure to afford 0.2 g (68%) of compound **6** as a brown solid. ^{1}H NMR (300 MHz, $CDCl_3$) δ 3.31 (s, 4H). HRMS (ESI) (M^+, $C_6H_4Br_2F_2N_2$) calcd 299.8709, found 299.8708.

Synthesis of Tributyl(4-hexylthiophen-2-yl)stannane, 7.[57] A solution of 3-hexylthiophene (1.5 g, 8.91 mmol) in anhydrous THF (35 mL) was cooled to −78 °C under nitrogen atmosphere. 6.73 mL of *n*-BuLi (1.6 M in hexane) was added dropwise to the solution and the reaction mixture was allowed to warm up to room temperature and stirred for 2 h. After that, the solution was cooled to 0 °C and 2.4 mL (8.91 mmol) of tributyltin chloride was added. After being stirred for 2 h, the mixture was poured into water and diluted with hexane to extract with brine. The organic phase was dried over $MgSO_4$ and the solvent was removed under reduced pressure. The resulting yellow oil was purified by column chromatography on silica gel to afford 2.5 g (61%) of compound **7** as yellow liquid. ^{1}H NMR (300 MHz, $CDCl_3$) δ 7.20−7.16 (m, 1H), 7.01−6.92 (m, 1H), 2.69−2.62 (m, 2H), 1.70−1.49 (m, 8H), 1.41−1.26 (m, 12), 1.21−0.96 (m, 6H), 0.95−0.85 (m,12H). HRMS (ESI) (M^+, $C_{22}H_{42}SSn$) calcd 458.2029, found 458.2021.

Synthesis of 5,8-Dibromo-6,7-difluoro-2,3-bis(3-hexyloxyphenyl)quinoxaline, 8. A mixture of compound **6** (3.61 g, 10.0 mmol), iron powder (6.70 g, 120.0 mmol), and acetic acid (60 mL) was stirred at 50 °C for 4 h. After filtering, compound **2** (4.10 g, 10.0 mmol) was added to the filtrate, followed by heating under reflux for 8 h. After that, the reaction mixture was poured into water, extracted with dichloromethane, and dried with anhydrous $MgSO_4$. The solvent was then removed via rotary evaporation and subsequently purified by column chromatography on silica gel using dichloromethane/hexane (1:7, v/v) as eluent to afford 4 g (59%) of compound **8** as a white solid. ^{1}H NMR (300 MHz, $CDCl_3$) δ 7.24−7.18 (m, 4H), 7.15−7.12 (m, 2H), 6.94−6.91 (m, 2H), 3.83 (t, J = 6.4 Hz, 4H), 1.70 (m, 4H), 1.42−1.35 (m, 4H), 1.34−1.24 (m, 8H), 0.89 (t, J = 7.2 Hz, 6H). ^{13}C NMR (75 MHz, $CDCl_3$) δ 194.52, 159.62, 134.21, 129.95,122.91, 122.19, 113.62, 68.35, 31.51, 29.05, 25.63, 22.55, 13.98. HRMS (ESI) (M^+, $C_{32}H_{34}Br_2F_2N_2O_2$) calcd 674.0955, found 674.0960.

Synthesis of 5,6-Difuoro-4,7-di(thiophen-2-yl)benzo[*c*]-[1,2,5]-thiadiazole, 9. A mixture of compound **7** (0.845 g, 1.85 mmol), compound **8** (0.5 g, 0.74 mmol), and $PdCl_2(PPh_3)_2$ (51.9 mg, 0.074 mmol) in toluene (30 mL) was heated under reflux for 48 h under nitrogen atmosphere. After the reaction, the solvent was removed under reduced pressure and the crude product was subsequently purified by column chromatography on silica gel to afford 0.25 g (40%) of compound **9** as an orange solid. ^{1}H NMR (300 MHz, $CDCl_3$) δ 8.03 (d, J = 3.6 Hz, 2H), 7.60 (dd, J = 5.2, 1.2 Hz, 2H), 7.34 (s, 2H), 7.24−7.22 (m, 6H), 6.95−6.92 (m, 2H), 3.89 (t, J = 6.4 Hz, 4H), 1.76−1.71 (m, 4H), 1.45−1.40 (m, 4H), 1.34−1.31 (m, 8H), 0.91 (t, J = 6.8 Hz, 6H). ^{13}C NMR (75 MHz, $CDCl_3$) δ 159.06, 151.33, 139.28, 134.70, 130.88, 130.78, 129.86, 129.20, 126.5, 122.76,

DOI: 10.1021/jacs.5b06710
J. Am. Chem. Soc. 2015, 137, 10420−10429

117.92, 116.62, 115.71, 68.16, 31.52, 29.10, 25.70, 22.62, 14.01. MALDI-MS m/z 850.08 (M^+).

Synthesis of 5,8-Bis(5-bromothiophen-2-yl)-6,7-difluoro-2,3-bis(3-hexyloxyphenyl)quinoxaline, 10. Compound **9** (156 mg, 0.18 mmol) was dissolved in 8 mL of DMF under nitrogen atmosphere and then *n*-bromosuccinimide (75 mg, 0.42 mmol) was added into the mixture in one portion. The mixture was stirred in the dark for 12 h and then the mixture was poured into water, diluted with CH_2Cl_2, and extracted with brine. The organic extract was separated ad dried over anhydrous $MgSO_4$. The solvent was removed via rotary evaporation and subsequently purified by column chromatography on silica gel to afford 111 mg (61%) of compound **10** as a red solid. ^{1}H NMR (300 MHz, $CDCl_3$) δ 7.76 (d, J = 4.0 Hz, 2H), 7.50−7.49 (m, 2H), 7.19 (t, J = 7.6 Hz, 2H), 7.14 (d, J = 4.4 Hz, 2H), 7.06−7.04 (m, 2H), 6.98−6.95 (m, 2H), 4.02 (t, J = 6.8 Hz, 4H), 1.82−1.75 (m, 4H), 1.50−1.44 (m, 4H), 1.37−1.31 (m, 8H), 0.92−0.88 (m, 6H). ^{13}C NMR (75 MHz, $CDCl_3$) δ 159.41, 151.67, 138.75, 133.91, 132.41, 130.90, 129.37, 129.11, 122.90. MALDI-MS m/z 1006.24 (M^+).

General Procedures of Polymerization.[57] Suzuki coupling reaction was used to synthesize the copolymers as shown in Scheme 1. In a 100 mL flask, monomer **10 or 11 or 12 or 13** (0.45 mmol-0.5 mmol), monomer **14** (0.5 mmol), and monomer **15** (0−0.05 mmol) were dissolved in 10 mL of toluene, and then 4−6 mg (0.02 mmol) of tetra-*n*-butylammonium bromide (Bu_4NBr) and 3 mL of Na_2CO_3 (2 M) was added. The mixture solution was purged with nitrogen for 1 h. After that, the mixture solution was degassed and refilled with N_2 (repeated 4 times) before and after the addition of $Pd(PPh_3)_4$ (7 mg, 0.006 mmol). The reactants were stirred at 100 °C for 48 h and then 50 mg of phenylboronic acid dissolved in 1 mL of THF was added. After 2 h, 0.5 mL of bromobenzene was added and further stirred for 3 h. The mixture was poured into 120 mL of methanol. The precipitate was filtered, washed with methanol and acetone to remove monomers, small oligomers, and inorganic salts. The crude product was dissolved in CH_2Cl_2 and then extracted with brine for 3 times. The organic extract was separated, dried over $MgSO_4$, and the solvent was removed under reduced pressure. The crude polymers were reprecipitated in $CHCl_3$/methanol and washed with acetone. Finally, the product was collected by filtration to afford 120−150 mg of polymer **PF-TC6FQ**, **PF-TTFQ**, **PF-TFQ**, or **PF-TQ**. GPC: PF-TC6FQ M_n: 25995, M_w: 44627, PDI: 1.72; PF-TFQ M_n: 13347, M_w: 31026, PDI: 2.32; PF-TTFQ M_n: 12199, M_w: 51200, PDI: 4.19; PF-TQ M_n: 8779, M_w: 28415, PDI: 3.24.

Synthesis of Folate-PEG-NH$_2$.[71] Folic acid (260 mg, 0.58 mmol)) was completely dissolved in 15 mL of DMSO under ultrasonication. Dicyclhexylcarbodiimide (74 mg, 0.65 mmol) and *N*-hydroxysuccinimide (134 mg, 0.65 mmol) was then added and the mixture was stirred in the dark for 12 h. After the reaction, the precipitate was filtered out using a hydrophilic 0.2 μm PTFE membrane filter and the filtrate was added into the acetone-ether (3:7) mixture solution. The solid was collected by centrifugation and washed with acetone and ether several times to obtain 511 mg of Folate-NHS ester as a yellow solid, which was used immediately for the next step. MALDI-MS m/z 539.91 (M^+). Folate-NHS ester (511 mg, 0.95 mmol) was dissolved fully in 15 mL of DMSO. 2.1 mL of 3,3′-oxybis(ethyleneoxy)bis(propylamine) and 102 mL of pyridine was added to the solution in sequence. The mixture was stirred in the dark for 8 h and then 2−3 mL of acetonitrile was added to solution to obtain a yellow precipitate. The precipitate was collected and washed with acetone to yield 148 mg (48%) of Folate-PEG-NH$_2$. MALDI-MS m/z 644.79 (M^+). Folate-PEG-NH$_2$ can be dissolved in DMSO and stored at 4 °C as a stock solution, while Folate-PEG-NH$_2$ solid should be stored at −20 °C.

Preparation of Quinoxaline-Based Pdots. Typically, 200 μL of copolymer solution (1 mg/mL in THF) and 0−20 μL of PS−PEG-COOH (2 mg/mL in THF) were added into 5 mL of THF. This mixture solution was then quickly injected into 10 mL of water under vigorous sonication. After that, THF was removed by purging with nitrogen on a 96 °C hot plate for 60 min. The resulting Pdot solution was filtered through a 0.2 μm cellulose membrane filter to remove any aggregates formed during Pdot preparation.

Bioconjugation and Characterization of Pdots. Bioconjugation was performed by using the EDC-catalyzed reaction between carboxylate-functionalized quinoxaline-based Pdots and the respective amine-containing streptavidin. In a typical bioconjugation reaction, 80 μL of polyethylene glycol (5% w/v PEG, MW 3350) and 80 μL of concentrated HEPES buffer (1 M) were added to 4 mL of Pdot solution, resulting in a Pdot solution in 20 mM HEPES buffer with a pH of 7.3. Then 240 μL of streptavidin (1 mg/mL) was added to the solution and mixed well on a vortex. After that, 80 μL of freshly prepared EDC solution (5 mg/mL in Milli-Q water) was added to the solution, and the mixture was stirred for 4 h at room temperature. After bionconjugation, 80 μL of BSA (10 wt %) was added to the Pdot solution and the reaction was continued for another 20 min. A 80-μL aliquot of Triton X-100 in Milli-Q water (2.5 wt %) was added to the Pdot-streptavidin mixture. The mixture was then transferred to a centrifugal ultrafiltration tube (Amicon Ultra-4, MWCO: 100 kDa), and then concentrated to 0.5 mL by centrifugation. Finally, the Pdot-streptavidin bioconjugates were purified by gel filtration using Sephacryl HR-300 gel media.

The average particle size was determined by dynamic light scattering and transmission electron microscopy (TEM). TEM images of the synthesized Pdots were acquired using a JEOL 2100 transmission electron microscope at an acceleration voltage of 200 kV. For TEM, a drop of Pdot aqueous solution was placed onto a carbon-coated grid and allowed to evaporate at room temperature. The absorption spectra of Pdots were measured using UV−visible spectroscopy (Dynamica Halo DB20S, Dynamica Scientific). The fluorescence spectra were collected using a Hitachi F-7000 fluorometer (Hitachi, Tokyo, Japan) under 450 nm excitation. Absolute fluorescence quantum yield of Pdots was determined by using an integrating sphere unit of Hitachi F-7000 fluorescence spectrophotometer.

Cell Culture and Labeling. The cervical cancer cell line HeLa and breast cancer cell line MCF-7 were ordered from Food Industry Research and Development Institute (Taiwan). Primary cultured HeLa cells were grown in Dulbecco's Modified Eagle Medium (cat. no. 11885, Invitrogen) supplemented with 10% fetal bovine serum (FBS) and 1% penicillin-streptomycin solution (5000 units/mL penicillin G, 50 μg/mL streptomycin sulfate in 0.85% NaCl) at 37 °C with 5% CO_2 humidified atmosphere. MCF-7 cells were cultured at 37 °C, 5% CO_2 in RPMI 1640 medium supplemented with 10% FBS and 1% penicillin-streptomycin solution. The cells were precultured in a T-25 flask and allowed to grow for 5−7 days prior to experiments until ∼80% confluence was reached. To prepare cell suspensions, the adherent cancer cells were quickly rinsed with media and then incubated in 0.8 mL of trypsin-ethylenediaminetetraacetic (EDTA) solution (0.25 w/v % trypsin, 0.25 g/L EDTA) at 37 °C for 3 min. The cell suspension solution was then centrifuged at 1000 rpm for 5 min to precipitate the cells to the bottom of the tube. After taking out the upper media, the cells was rinsed and resuspended in 5 mL of culture media. Approximately tens of thousands cells were split onto a glass-bottomed culture dish and allowed to grow for 12 h before Pdot labeling. Prior to fluorescence imaging, the cells were rinsed with PBS buffer to remove any nonspecifically bound Pdots on the cell surface.

For cell labeling experiments, BlockAid blocking buffer was purchased from Invitrogen (Eugene, OR, USA). For labeling cell-surface markers with IgG, a million MCF-7 cells in 100-μL labeling buffer (1× PBS, 2 mM EDTA, 1% BSA) was incubated with 0.3 μL of 0.5 mg/mL primary biotin antihuman CD326 EpCAM antibody (BioLegend, San Diego, CA, USA) on a rotary shaker in the dark and at room temperature for 30 min, followed by a washing step using labeling buffer. Then the cells were incubated with 1.5 nM Pdot-streptavidin conjugates in BlockAid buffer for 30 min on a shaker in the dark and at room temperature, followed by two washing steps with labeling buffer. Prior to cell incubation, Pdot solutions were sonicated for 3 min in order to disperse any potential aggregates. Negative controls were obtained by incubating cells with Pdot-streptavidin conjugates in the absence of primary biotinylated-antibody. Cell fixation was performed by dissolving the cell pellet obtained by

DOI: 10.1021/jacs.5b06710
J. Am. Chem. Soc. 2015, 137, 10420−10429

centrifugation in 500 μL of fixing buffer (1× PBS, 2 mM EDTA, 1% BSA, 1% PFA).

For microtubule-labeling experiments, tens of thousands of HeLa cells were plated on a 22 × 22 mm glass coverslip (Biogenesis, Taiwan) and cultured until the density reached 60−70% confluence. The cells were fixed with 4% paraformaldehyde for 15 min, permeabilized with 0.5% Triton-X 100 in PBS buffer for 15 min, and then blocked in BlockAid blocking buffer for another 40 min. The fixed and blocked HeLa cells were subsequently incubated with 2 μg/mL biotinylated monoclonal anti-α-tubulin antibody (BioLegend, San Diego, CA, USA) for 60 min, and then Pdot-streptavidin conjugates for 40 min. The Pdot labeled cells were then counterstained with Hoechst 34580 for 15 min and imaged immediately on a fluorescence confocal microscope (Nikon D-Eclipse C1).

Flow cytometry measurements were performed on fresh samples with 10^6 cells/0.5 mL and prepared following the procedure previously described. The flow cytometer CyFlow SL (Partec, Münster, Germany) was used: Cells flowing in the detection chamber were hit with a 488 nm laser beam, fluorescence emission were collected and filtered by a 590 long-pass, and all signals were detected by PMT arrays. Representative populations of cells were chosen by selection of an appropriate gate. Detection of cell fluorescence was continued until at least 104 events had been collected in the active gate.

Cell Imaging. The fluorescence spectra of Pdot-tagged cells were acquired with a fluorescence confocal microscope (Nikon D-Eclipse C1) under ambient conditions (24 ± 2 °C). The confocal fluorescence images were collected using a diode laser at 488 nm (~15 mW) as the excitation source and an integration time of 1.6 μs/pixel. A CF1 Plan Fluor 40x (N. A. 0.75, W.D. 0.66 mm) objective was utilized for imaging and spectral data acquisition; the laser was focused to a spot size of ~7 μm^2. The blue fluorescence was collected by filtering through a 450/35 band-pass (λ_{ex} = 408 nm) while the red fluorescence was collected by filtering through a 570 long-pass (λ_{ex} = 488 nm).

MTT Assay. The cellular cytotoxicity of the Pdots was examined on HeLa cells. The number of viable cells was determined using the MTT assay with 3-(4,5-dimethylthiazole-2-yl)-2,5-phenyltetrazolium bromide. HeLa cells were first seeded in each well of a 24-well culture plate and then incubated with various concentrations of Pdots (100 pM, 200 pM, and 400 pM) for 6, 12, and 24 h. After that, 20 μL (5 mg/mL) of MTT aqueous solution was added to each well and the cells were further incubated for 4 h at 37 °C to deoxidize MTT. The medium was then washed out and 300 μL of DMSO was added into each well to dissolve formazam crystals. Absorbance was measured by a BioTek ELx800 microplate reader at 570 nm, while the cells cultured with the pure medium (e.g., without Pdots) served as controls.

In Vivo Imaging on Zebrafish. The transgenic zebrafish, *Tg(kdrl:eGFP)*^{la116}[72] expressing eGFP in the endothelial cells,[72] were maintained at 28 °C and bred under standard conditions with approval from National SunYat-sen University Animal Care Committee. For angiography imaging, 37 nL Pdots (125 nM) in 20 mM HEPES buffer was injected into the sinus venosus of the anaesthetized zebrafish embryos 3 days post fertilization (dpf) with 5% (v/v) tricaine (Sigma). The injected embryos were recovered for 30 min, immobilized in 1.5% low melting point agarose (invitrogen), and then imaged immediately using a fluorescence confocal microscope (Nikon D-Eclipse C1). The green fluorescence was collected by filtering through a 515/30 band-pass (λ_{ex} = 488 nm) while the red fluorescence was collected by filtering through a 570 long-pass (λ_{ex} = 488 nm).

■ ASSOCIATED CONTENT

Supporting Information

The Supporting Information is available free of charge on the ACS Publications website at DOI: 10.1021/jacs.5b06710.

Additional information as noted in text. (PDF)

■ AUTHOR INFORMATION

Corresponding Author

*yhchan@mail.nsysu.edu.tw

Notes

The authors declare no competing financial interest.

■ ACKNOWLEDGMENTS

We would like to thank the Ministry of Science (103-2113-M-110-004-MY2) and National Sun Yat-sen University. We also gratefully acknowledge support from Prof. Chao-Ming Chiang, Prof. Wei-Lung Tseng, Prof. Chin-Hsing Chou, and Dr. Ying-Hsiao Chen from National Taiwan University. We especially thank Dr. Fangmao Ye for the measurements of single-particle fluorescence brightness.

■ REFERENCES

(1) Hell, S. W.; Wichmann, J. *Opt. Lett.* **1994**, *19*, 780.
(2) Rittweger, E.; Han, K. Y.; Irvine, S. E.; Eggeling, C.; Hell, S. W. *Nat. Photonics* **2009**, *3*, 144.
(3) Gustafsson, M. G. L. *Proc. Natl. Acad. Sci. U. S. A.* **2005**, *102*, 13081.
(4) Rust, M. J.; Bates, M.; Zhuang, X. *Nat. Methods* **2006**, *3*, 793.
(5) Betzig, E.; Patterson, G. H.; Sougrat, R.; Lindwasser, O. W.; Olenych, S.; Bonifacino, J. S.; Davidson, M. W.; Lippincott-Schwartz, J.; Hess, H. F. *Science* **2006**, *313*, 1642.
(6) Huang, B.; Bates, M.; Zhuang, X. *Annu. Rev. Biochem.* **2009**, *78*, 993.
(7) Sengupta, P.; Engelenburg, S. B. v.; Lippincott-Schwartz, J. *Chem. Rev.* **2014**, *114*, 3189.
(8) Fernández-Suárez, M.; Ting, A. Y. *Nat. Rev. Mol. Cell Biol.* **2008**, *9*, 929.
(9) Orrit, M. *Nat. Photonics* **2014**, *8*, 887.
(10) Frangioni, J. V. *J. Clin. Oncol.* **2008**, *26*, 4012.
(11) Chi, C.; Du, Y.; Ye, J.; Kou, D.; Qiu, J.; Wang, J.; Tian, J.; Chen, X. *Theranostics* **2014**, *4*, 1072.
(12) Dam, G. M. v.; Themelis, G.; Crane, L. M. A.; Harlaar, N. J.; Pleijhuis, R. G.; Kelder, W.; Sarantopoulos, A.; Jong, J. S. d.; Arts, H. J. G.; Zee, A. G. J. v. d.; Bart, J.; Low, P. S.; Ntziachristos, V. *Nat. Med.* **2011**, *17*, 1315.
(13) Vahrmeijer, A. L.; Hutteman, M.; Vorst, J. R. v. d.; Velde, C. J. H. v. d.; Frangioni, J. V. *Nat. Rev. Clin. Oncol.* **2013**, *10*, 507.
(14) Sevick-Muraca, E. M.; Houston, J. P.; Gurfinkel, M. *Curr. Opin. Chem. Biol.* **2002**, *6*, 642.
(15) Ntziachristos, V.; Bremer, C.; Weissleder, R. *Eur. Radiol.* **2003**, *13*, 195.
(16) Bae, S. W.; Tan, W.; Hong, J.-I. *Chem. Commun.* **2012**, *48*, 2270.
(17) Yan, J.; Estéveza, M. C.; Smith, J. E.; Wang, K.; He, X.; Wang, L.; Tan, W. *Nano Today* **2007**, *2*, 44.
(18) Lee, J. E.; Lee, N.; Kim, H.; Kim, J.; Choi, S. H.; Kim, J. H.; Kim, T.; Song, I. C.; Park, S. P.; Moon, W. K.; Hyeon, T. *J. Am. Chem. Soc.* **2010**, *132*, 552.
(19) Reul, R.; Tsapis, N.; Hillaireau, H.; Sancey, L.; Mura, S.; Recher, M.; Nicolas, J.; Collcd, J.-L.; Fattal, E. *Polym. Chem.* **2012**, *3*, 694.
(20) Yang, Y.; An, F.; Liu, Z.; Zhang, X.; Zhou, M.; Li, W.; Hao, X.; Lee, C.-s.; Zhang, X. *Biomaterials* **2012**, *33*, 7803.
(21) Medintz, I. L.; Uyeda, H. T.; Goldman, E. R.; Mattoussi, H. *Nat. Mater.* **2005**, *4*, 435.
(22) Somers, R. C.; Bawendi, M. G.; Nocera, D. G. *Chem. Soc. Rev.* **2007**, *36*, 579.
(23) Michalet, X.; Pinaud, F. F.; Bentolila, L. A.; Tsay, J. M.; Doose, S.; Li, J. J.; Sundaresan, G.; Wu, A. M.; Gambhir, S. S.; Weiss, S. *Science* **2005**, *307*, 538.
(24) Peng, J.; He, X.; Wang, K.; Tan, W.; Wang, Y.; Liu, Y. *Anal. Bioanal. Chem.* **2007**, *388*, 645.
(25) Peng, H.-s.; Stolwijk, J. A.; Sun, L.-N.; Wegener, J.; Wolfbeis, O. S. *Angew. Chem., Int. Ed.* **2010**, *49*, 4246.
(26) Derfus, A. M.; Chan, W. C. W.; Bhatia, S. N. *Nano Lett.* **2004**, *4*, 11.
(27) Brunetti, V.; Chibli, H.; Fiammengo, R.; Galeone, A.; Malvindi, M. A.; Vecchio, G.; Cingolani, R.; Nadeau, J. L.; Pompa, P. P. *Nanoscale* **2013**, *5*, 307.

DOI: 10.1021/jacs.5b06710
J. Am. Chem. Soc. 2015, 137, 10420−10429

(28) Tsoi, K. M.; Dai, Q.; Alman, B. A.; Chan, W. C. W. *Acc. Chem. Res.* **2013**, *46*, 662.
(29) Wu, C.; Bull, B.; Szymanski, C.; Christensen, K.; McNeill, J. *ACS Nano* **2008**, *2*, 2415.
(30) Tian, Z.; Yu, J.; Wu, C.; Szymanski, C.; McNeill, J. *Nanoscale* **2010**, *2*, 1999.
(31) Pecher, J.; Mecking, S. *Chem. Rev.* **2010**, *110*, 6260.
(32) Kaeser, A.; Schenning, A. P. H. J. *Adv. Mater.* **2010**, *22*, 2985.
(33) Tuncel, D.; Demir, H. V. *Nanoscale* **2010**, *2*, 484.
(34) Li, K.; Liu, B. *J. Mater. Chem.* **2012**, *22*, 1257.
(35) Pu, K.-Y.; Liu, B. *Adv. Funct. Mater.* **2011**, *21*, 3408.
(36) Wu, C.; Chiu, D. T. *Angew. Chem., Int. Ed.* **2013**, *52*, 3086.
(37) Wu, C.; Hansen, S. J.; Hou, Q.; Yu, J.; Zeigler, M.; Jin, Y.; Burnham, D. R.; McNeill, J. D.; Olson, J. M.; Chiu, D. T. *Angew. Chem., Int. Ed.* **2011**, *50*, 3430.
(38) Chan, Y.-H.; Wu, C.; Ye, F.; Jin, Y.; Smith, P. B.; Chiu, D. T. *Anal. Chem.* **2011**, *83*, 1448.
(39) Chan, Y.-H.; Jin, Y.; Wu, C.; Chiu, D. T. *Chem. Commun.* **2011**, *47*, 2820.
(40) Ye, F.; Wu, C.; Jin, Y.; Chan, Y.-H.; Zhang, X.; Chiu, D. T. *J. Am. Chem. Soc.* **2011**, *133*, 8146.
(41) Wu, C.; Schneider, T.; Zeigler, M.; Yu, J.; Schiro, P. G.; Burnham, D. R.; McNeill, J. D.; Chiu, D. T. *J. Am. Chem. Soc.* **2010**, *132*, 15410.
(42) Wu, P.-J.; Chen, J.-L.; Chen, C.-P.; Chan, Y.-H. *Chem. Commun.* **2013**, *49*, 898.
(43) Chen, C.-P.; Wu, P.-J.; Lioua, S.-Y.; Chan, Y.-H. *RSC Adv.* **2013**, *3*, 17507.
(44) Chan, Y.-H.; Wu, P.-J. *Part. Part. Syst. Charact.* **2015**, *32*, 11.
(45) Massey, M.; Wu, M.; Conroy, E. M.; Algar, W. R. *Curr. Opin. Biotechnol.* **2015**, *34*, 30.
(46) Chang, K.; Liu, Z.; Chen, H.; Sheng, L.; Zhang, S. X.-A.; Chiu, D. T.; Yin, S.; Wu, C.; Qin, W. *Small* **2014**, *10*, 4270.
(47) Sun, K.; Chen, H.; Wang, L.; Yin, S.; Wang, H.; Xu, G.; Chen, D.; Zhang, X.; Wu, C.; Qin, W. *ACS Appl. Mater. Interfaces* **2014**, *6*, 10802.
(48) Jin, Y.; Ye, F.; Zeigler, M.; Wu, C.; Chiu, D. T. *ACS Nano* **2011**, *5*, 1468.
(49) Zhang, X.; Yu, J.; Rong, Y.; Ye, F.; Chiu, D. T.; Uvdal, K. *Chem. Sci.* **2013**, *4*, 2143.
(50) Xiong, L.; Shuhendler, A. J.; Rao, J. *Nat. Commun.* **2012**, *3*, 1193.
(51) Yu, J.; Wu, C.; Zhang, X.; Ye, F.; Gallina, M. E.; Rong, Y.; Wu, I.-C.; Sun, W.; Chan, Y.-H.; Chiu, D. T. *Adv. Mater.* **2012**, *24*, 3498.
(52) Wu, P.-J.; Kuo, S.-Y.; Huang, Y.-C.; Chen, C.-P.; Chan, Y.-H. *Anal. Chem.* **2014**, *86*, 4831.
(53) Huang, Y.-C.; Chen, C.-P.; Wu, P.-J.; Kuo, S.-Y.; Chan, Y.-H. *J. Mater. Chem. B* **2014**, *2*, 6188.
(54) Kuo, S.-Y.; Li, H.-H.; Wu, P.-J.; Chen, C.-P.; Huang, Y.-C.; Chan, Y.-H. *Anal. Chem.* **2015**, *87*, 4765.
(55) Rong, Y.; Wu, C.; Yu, J.; Zhang, X.; Ye, F.; Zeigler, M.; Gallina, M. E.; Wu, I.-C.; Zhang, Y.; Chan, Y.-H.; Sun, W.; Uvdal, K.; Chiu, D. T. *ACS Nano* **2013**, *1*, 376.
(56) Wu, I.-C.; Yu, J.; Ye, F.; Rong, Y.; Gallina, M. E.; Fujimoto, B. S.; Zhang, Y.; Chan, Y.-H.; Sun, W.; Zhou, X.-H.; Wu, C.; Chiu, D. T. *J. Am. Chem. Soc.* **2015**, *137*, 173.
(57) Chen, C.-P.; Huang, Y.-C.; Liou, S.-Y.; Wu, P.-J.; Kuo, S.-Y.; Chan, Y.-H. *ACS Appl. Mater. Interfaces* **2014**, *6*, 21585.
(58) Chen, H.-C.; Chen, Y.-H.; Liu, C.-C.; Chien, Y.-C.; Chou, S.-W.; Chou, P.-T. *Chem. Mater.* **2012**, *24*, 4766.
(59) Seo, J.; Bonneau, C.; Matsuda, R.; Takata, M.; Kitagawa, S. *J. Am. Chem. Soc.* **2011**, *133*, 9005.
(60) Dang, D.; Chen, W.; Yang, R.; Zhu, W.; Mammo, W.; Wang, E. *Chem. Commun.* **2013**, *49*, 9335.
(61) Chen, H.-C.; Chen, Y.-H.; Liu, C.-H.; Hsu, Y.-H.; Chien, Y.-C.; Chuang, W.-T.; Cheng, C.-Y.; Liu, C.-L.; Chou, S.-W.; Tung, S.-H.; Chou, P.-T. *Polym. Chem.* **2013**, *4*, 3411.
(62) Wu, H.; Qu, B.; Cong, Z.; Liu, H.; Tian, D.; Gao, B.; An, Z.; Gao, C.; Xiao, L.; Chen, Z.; Liu, H.; Gong, Q.; Wei, W. *React. Funct. Polym.* **2012**, *72*, 897.
(63) Zhang, X.; Yu, J.; Wu, C.; Jin, Y.; Rong, Y.; Ye, F.; Chiu, D. T. *ACS Nano* **2012**, *6*, 5429.
(64) Price, S. C.; Stuart, A. C.; Yang, L.; Zhou, H.; You, W. *J. Am. Chem. Soc.* **2011**, *133*, 4625.
(65) Zhang, Y.; Yu, J.; Gallina, M. E.; Sun, W.; Rong, Y.; Chiu, D. T. *Chem. Commun.* **2013**, *49*, 8256.
(66) Liu, Z.; Sun, Z.; Di, W.; Qin, W.; Yuan, Z.; Wu, C. *Opt. Lett.* **2015**, *40*, 1242.
(67) Lieschke, G. J.; Currie, P. D. *Nat. Rev. Genet.* **2007**, *8*, 353.
(68) Qin, W.; Ding, D.; Liu, J.; Yuan, W. Z.; Hu, Y.; Liu, B.; Tang, B. Z. *Adv. Funct. Mater.* **2012**, *22*, 771.
(69) Liu, J.; Geng, J.; Liao, L.-D.; Thakor, N.; Gao, X.; Liu, B. *Polym. Chem.* **2014**, *5*, 2854.
(70) Li, K.; Liu, B. *Chem. Soc. Rev.* **2014**, *43*, 6570.
(71) Dhar, S.; Liu, Z.; Thomale, J.; Dai, H.; Lippard, S. J. *J. Am. Chem. Soc.* **2008**, *130*, 11467.
(72) Choi, J.; Dong, L.; Ahn, J.; Dao, D.; Hammerschmidt, M.; Chen, J.-N. *Dev. Biol.* **2007**, *304*, 735.
(73) Bouteiller, C.; Clavé, G.; Bernardin, A.; Chipon, B.; Massoneau, M.; Renard, P.-Y.; Romieu, A. *Bioconjugate Chem.* **2007**, *18*, 1303.

DOI: 10.1021/jacs.5b06710
J. Am. Chem. Soc. 2015, 137, 10420−10429